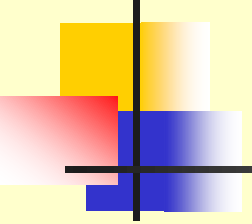


Properties of short GRBs with structured jet

Daming Wei

Purple Mountain Observatory

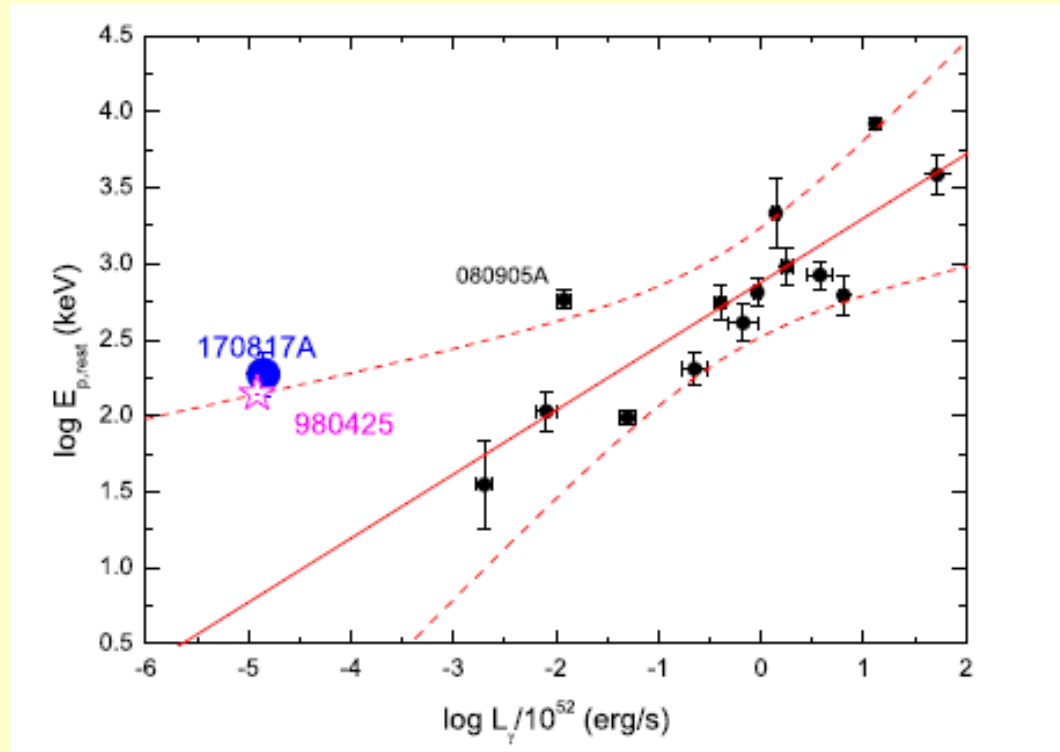
Collaborators: Jin, Z.P., Fan, Y.Z., Guo, Q., Yue, C., Li, X., Wang, H.,
Duan, K.K.



outline

- Properties of sGRBs with structured jet
- Statistical properties of GRBs
- Kilonova
- Summary

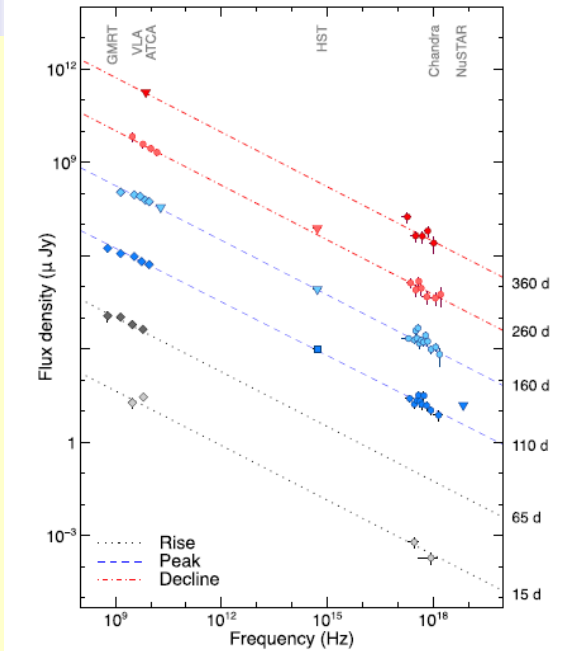
The E_p -L relation



(Wang et al. 2017)

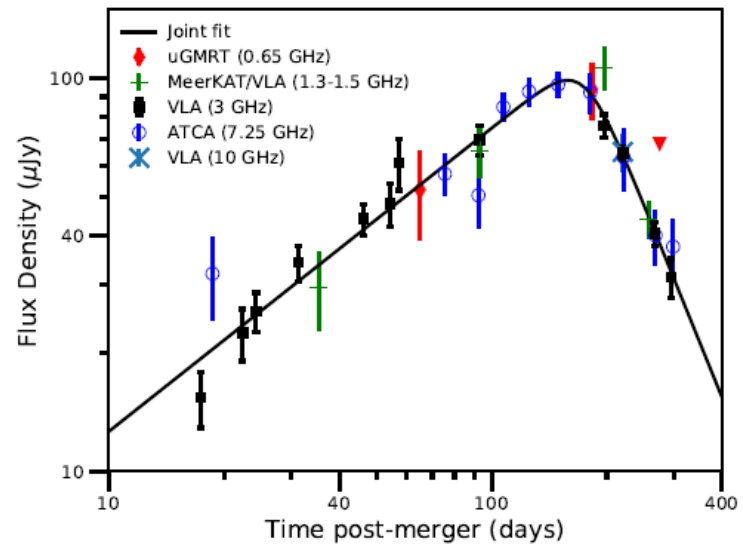
GRB 170817A does not follow the regular correlations.

Jet signature of GRB 170817A



(Troja et al. 2018)

spectral index $\beta \sim -0.6$,
electron index $p \sim 2.2$



(Mooley et al. 2018)

temporal decay index $\alpha \sim -2.2$

Structured jet

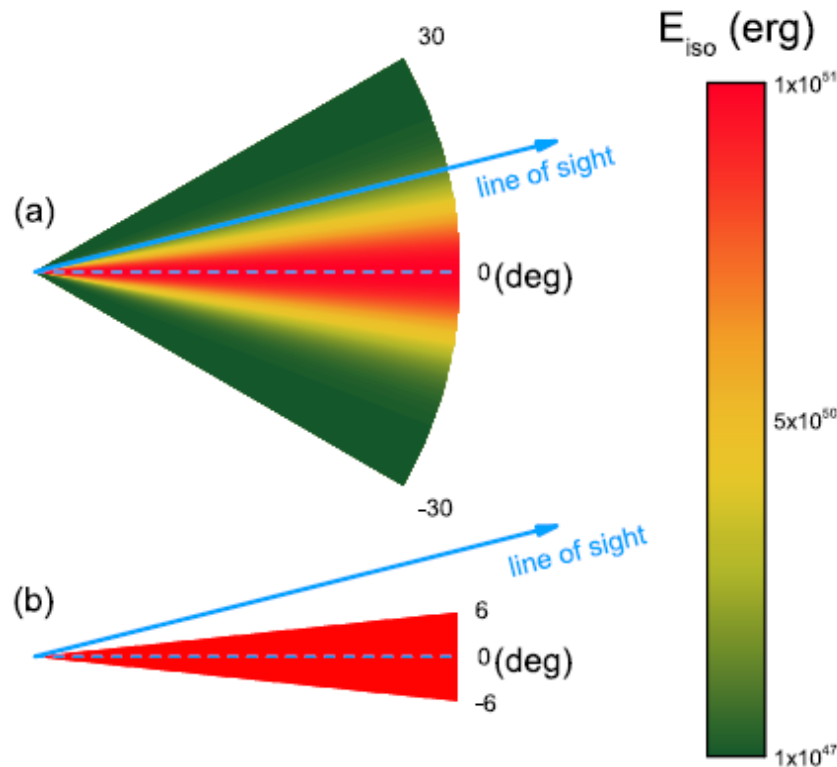
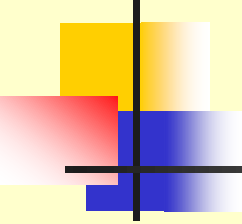


Figure 8. (a) Illustration of the off-axis scenario in the structured jet model. (b) Illustration of the off-beam scenario in the uniform jet model.

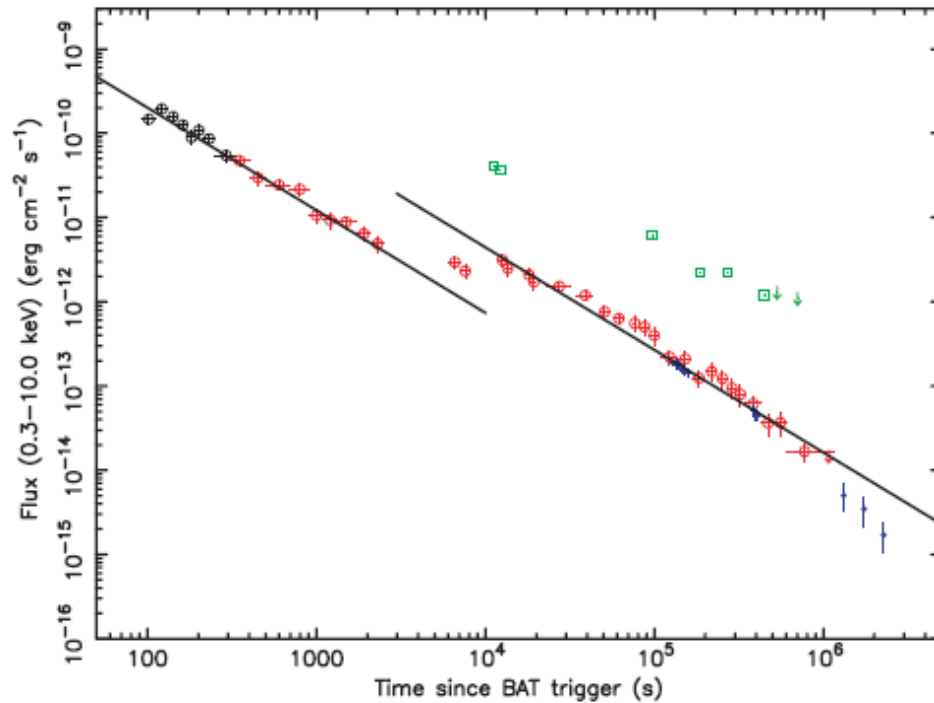
can be seen for
relative large angle

$\theta > \theta_j$, flux drop
very quickly

(Jin et al. 2018)

- 
-
- Besides GRB 170817A, are there any other short GRBs show evidence of structured jet?

One example: GRB 051221A



$T_{90} \sim 1.4\text{s}$
 $E_{\text{peak}} \sim 400\text{ KeV}$
 $z=0.5464$
 $\alpha_1 \sim 1.16$
 $\alpha_3 \sim 1.09$
 $\alpha_2 \sim 0.04$

(Burrows et al. 2006)

The X-ray afterglow of short GRB 051221A

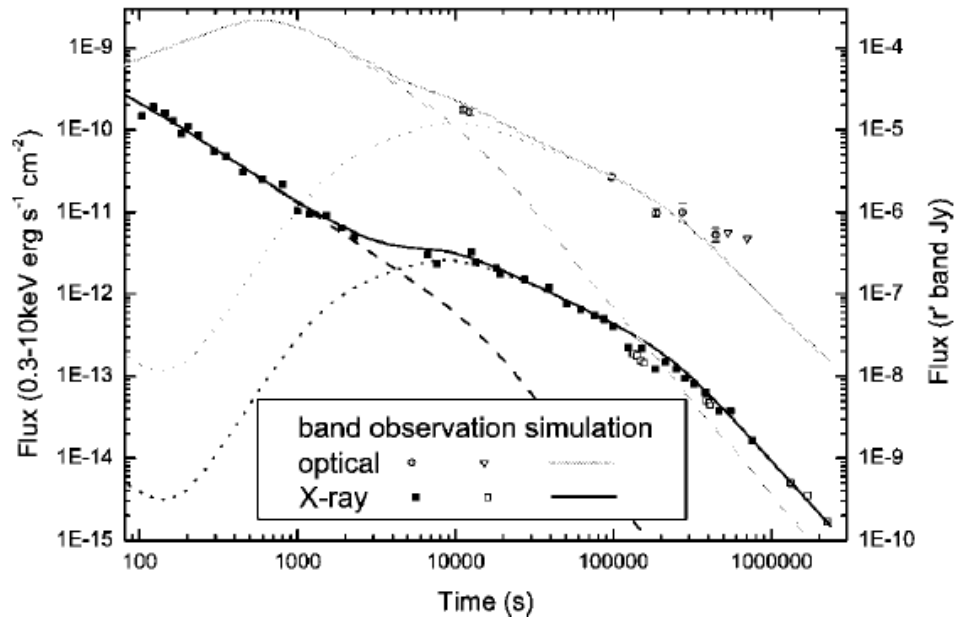
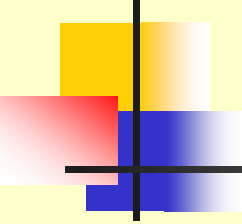
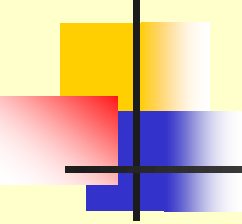


FIG. 2.—Fit to the multiband afterglow of GRB 051221A. Circles and squares are optical (r' band) and X-ray (0.3–10 keV) observations, respectively. The dashed, dotted, and solid lines are narrow, wide jet, and combined calculation, respectively.

(Jin et al. 2007)

The X-ray afterglow flat segment of short GRB 051221A can be well reproduced by two-component jet model.

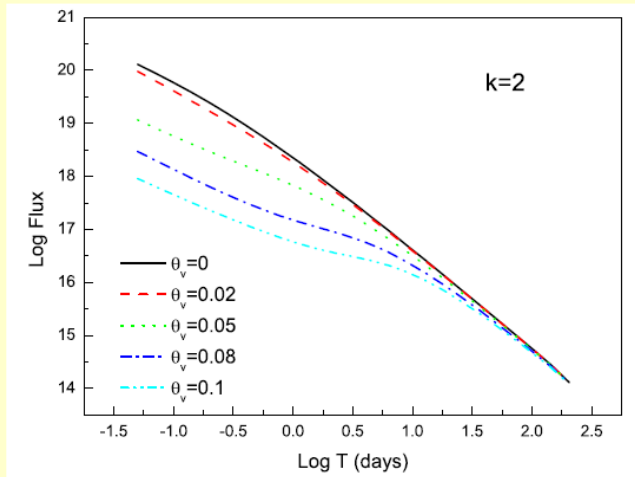
- 
-
- Whether GW170817-like mergers are indeed the source of the bright sGRBs?
 - Need to look for direct link between GW170817/GRB 170817A and other bright sGRBs



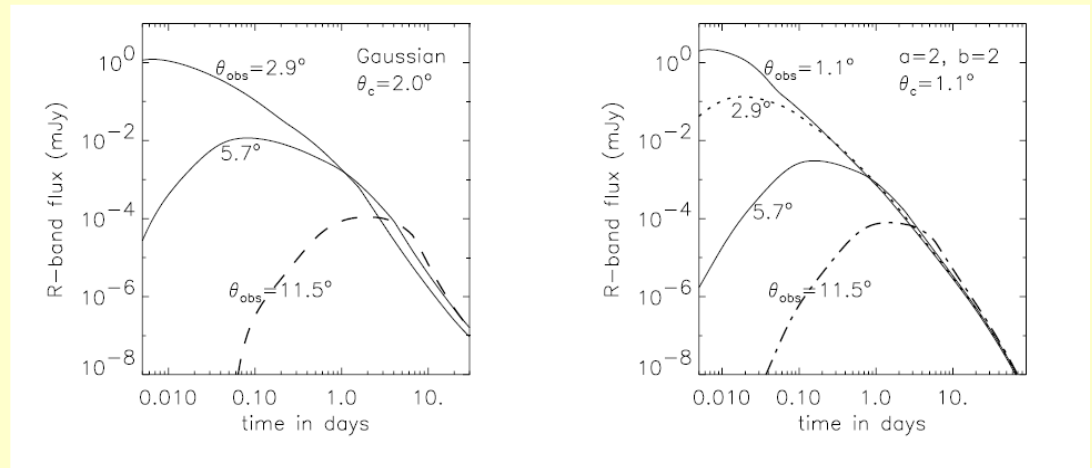
The structured jet model

- The structured jet model has been investigated by many papers (e.g. Meszaros et al. 1998; Dai & Gou 2001; Zhang & Meszaros 2002; Rossi et al. 2002; ...)
- The afterglow light curves will be affected by the jet structure (e.g. Wei & Jin 2003; Kumar & Granot 2003; ...)

GRB afterglow light curves from structured jet



(Wei & Jin 2003)



(Kumar & Granot 2003)

If viewed off-axis, the early afterglow emission is quite different for different viewing angle, while at late time the afterglow emission are similar. $\alpha \sim p$

The X-ray afterglow of GRB170817A vs. other sGRBs

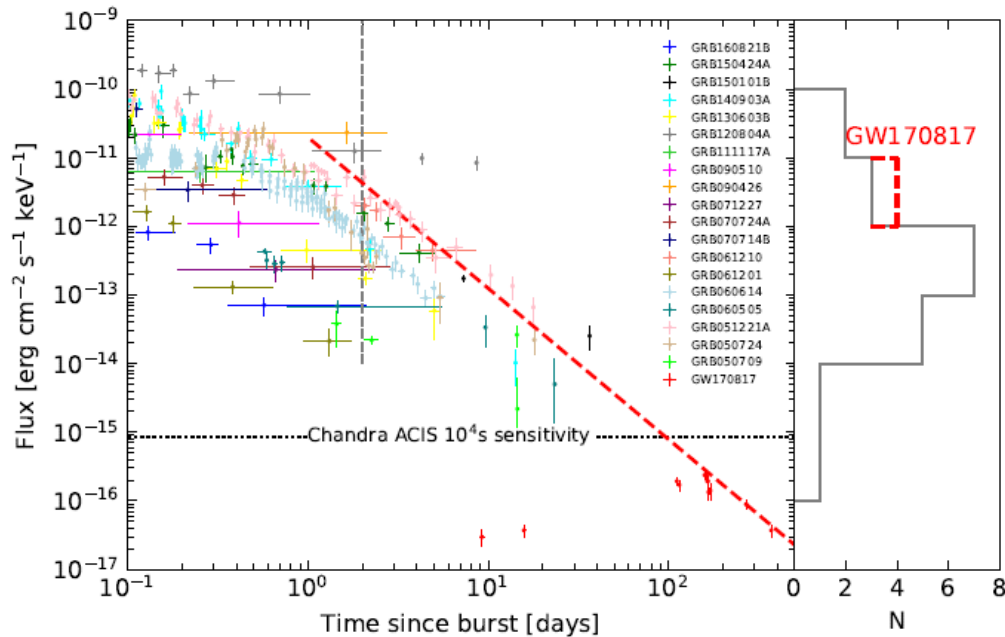


FIG. 1: The “long-lasting” X-ray (1.732 keV) afterglow emission of some sGRBs and GW170817/GRB 170817A[11, 27], if occurred at the same distance of 200 Mpc. The red dashed line represents the “on-axis” extrapolation to early times from the very late ($t > 150$ day) X-ray afterglow data of GRB 170817A, the vertical dashed line represents the time of 2 day after the burst,

(Duan et al. 2019)

Extrapolate the late X-ray afterglow data to early time. If viewed on-axis, the afterglow would be brighter than many other sGRBs.

The optical & radio afterglow

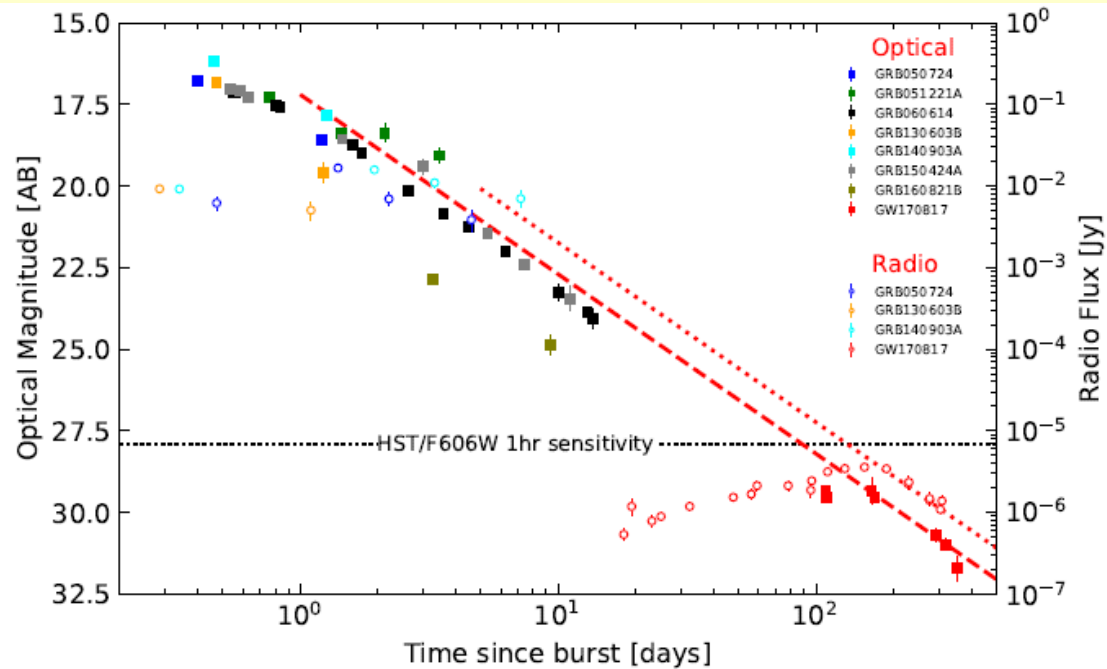
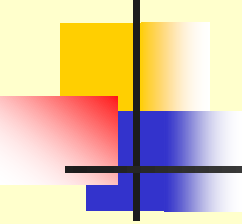


FIG. 2: The “long-lasting” R -band (the filled squares) and radio (6 GHz; the open circles) afterglow emission of some sGRBs and GW170817/GRB 170817A, if took place at the same distance of 200 Mpc. The HST sensitivity is from the Wide Field Camera 3 Instrument Handbook for Cycle 27

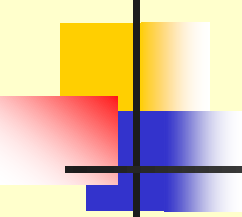
(Duan et al. 2019)

There is a tight connection between GW170817-like mergers and other bright sGRBs.



Nearby sGRBs

- It is expected that during aLIGO/Virgo O3 runs more 170817A-like events will be detected?
- Since the Advanced LIGO/Virgo can only detect gravitational signals from binary neutron star mergers or black hole-neutron star mergers at close distances, so the sGRBs associated with gravitational waves will be detected mainly at close distances.



Characteristics of sGRBs with SJ

- For structured jet, we use the Gaussian distribution to describe the luminosity and Lorentz factor distribution

$$L(\theta) = \frac{dE}{dt d\Omega} = \frac{L_0}{4\pi} e^{-(\theta^2/\theta_c^2)}$$

$$\Gamma(\theta) = 1 + (\Gamma_0 - 1) e^{-(\theta^2/\theta_c^2)}$$

- For sGRBs originating from the merging of binary compact objects, the formation rate of sGRBs

$$R_{GRB}(t) \propto \int_{t_F}^t dt' R_{SF}(t') P_m(t-t')$$

$$P_m(t) \propto t^\alpha$$

The formation rate of sGRBs

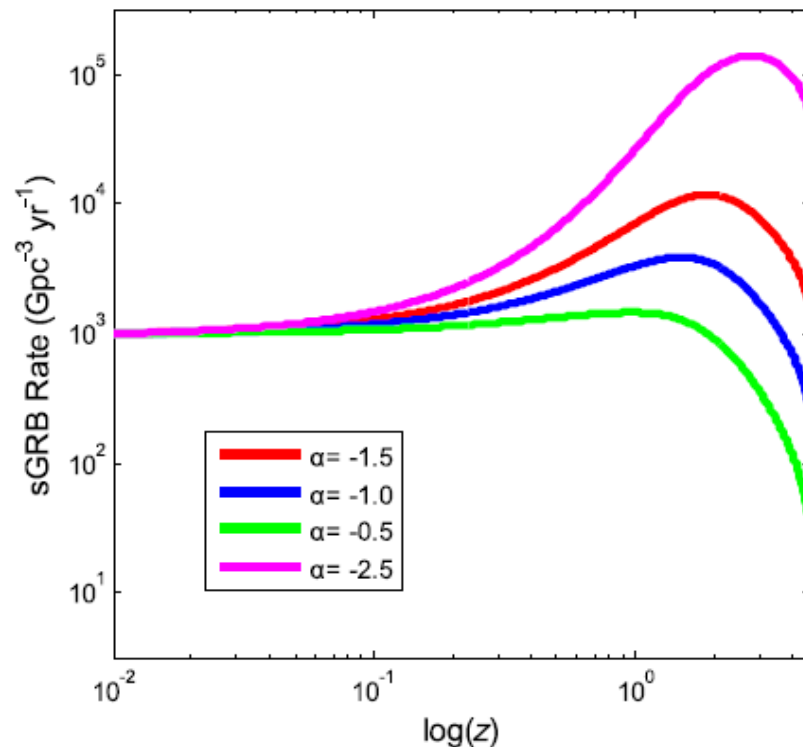


Figure 2. The formation rate history of sGRBs that is obtained with the assumption that they are associated with binary neutron star mergers. The rate of local NS–NS mergers is taken to be $\rho_0 = 1000 \text{ Gpc}^{-3} \text{ yr}^{-1}$ (Abbott et al. 2019). The green, blue, red, and purple lines correspond to different values of α with $\alpha = -0.5, -1.0, -1.5, -2.5$.

(Guo, Wei & Wang 2020)

The distribution of luminosity

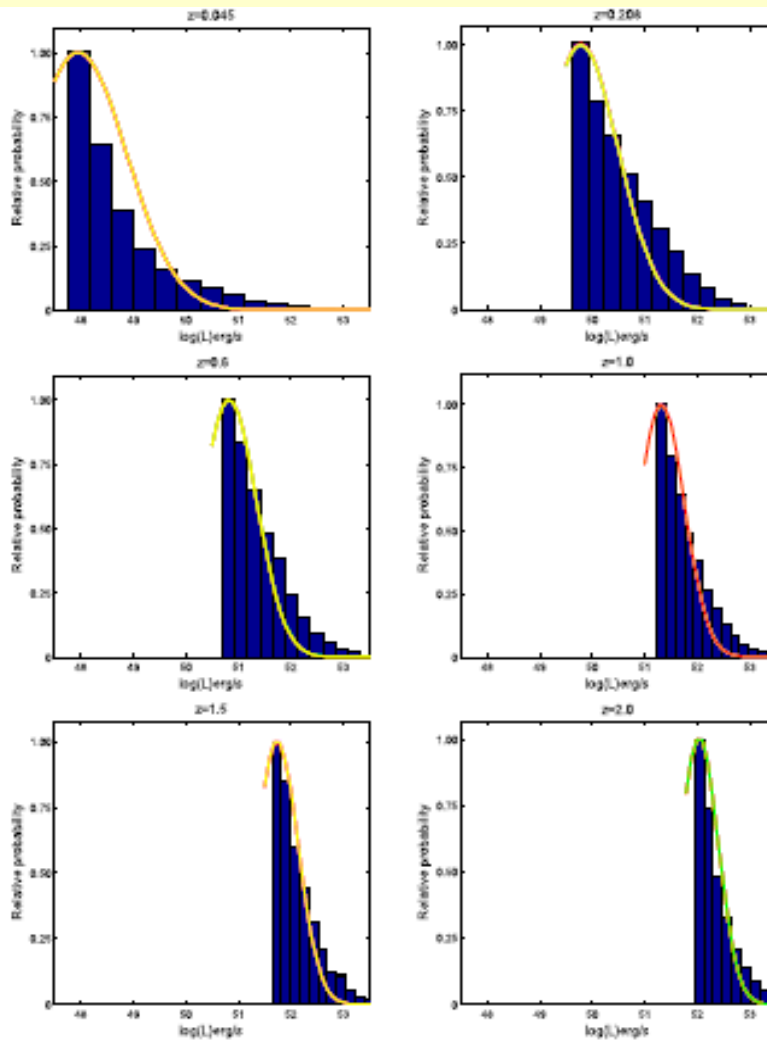
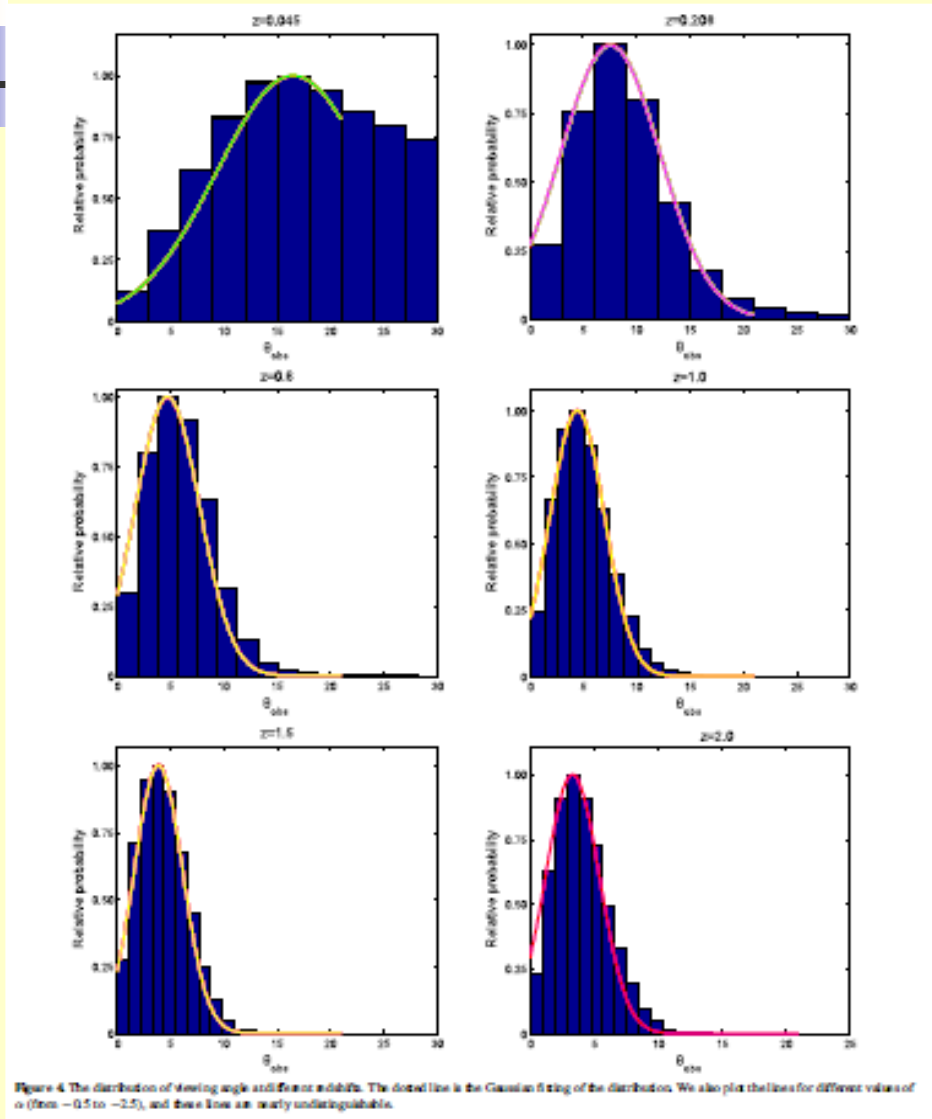


Figure 3. The distribution of luminosity at different redshifts. The dotted line is the Gaussian fitting of the distribution. Weak plot the line for different values of α (from -0.5 to -1.5), and these lines are nearly unrecognizable.

At $d=200$ Mpc,
 $L_p \sim 8 \times 10^{47} \text{ ergs}^{-1}$

(Guo, Wei & Wang 2020)

The distribution of viewing angle



At $d=200$ Mpc,
viewing angle $\sim 17^\circ$

The evolution of luminosity and viewing angle with redshift

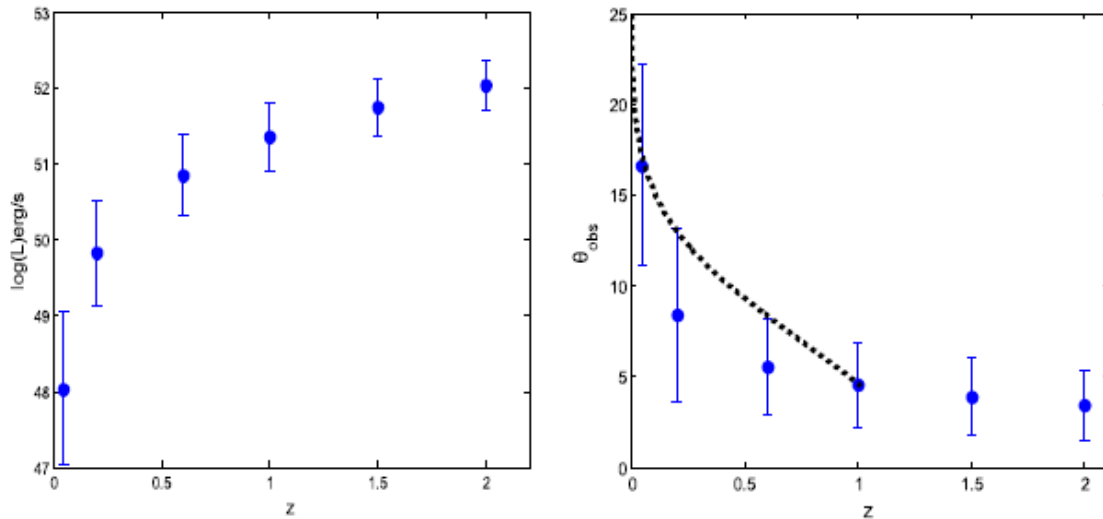


Figure 5. The evolution of the typical luminosity and viewing angle with redshift. The error bars are 1σ errors. The dashed line is the distribution of the maximum observable viewing angle obtained in Howell et al. (2019).

The observed typical luminosity increase with redshift, while the typical viewing angle decrease with redshift.

At smaller redshift the luminosity rise rapidly while at larger redshift (such as $z > 1$) they increase slowly.

Detection probability & normalized number distribution

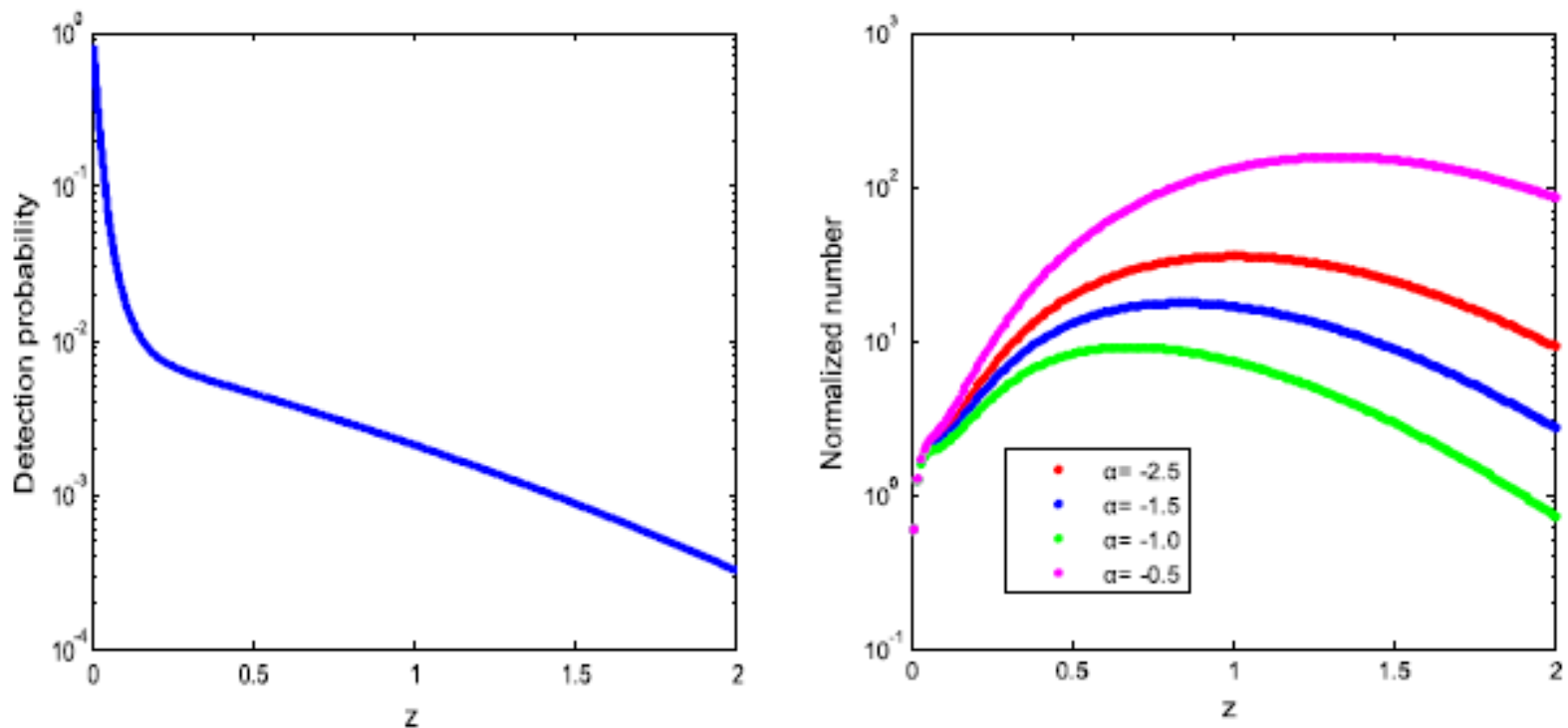


Figure 7. Left is the distribution of detection probability with redshift. Right is the normalized number distribution of observed sGRBs with our simulation, where the dotted lines are the 1σ uncertainty range. The green, blue, red, and purple lines correspond to different values of α with $\alpha = -0.5, -1.0, -1.5, -2.5$.

α inferred from simulation

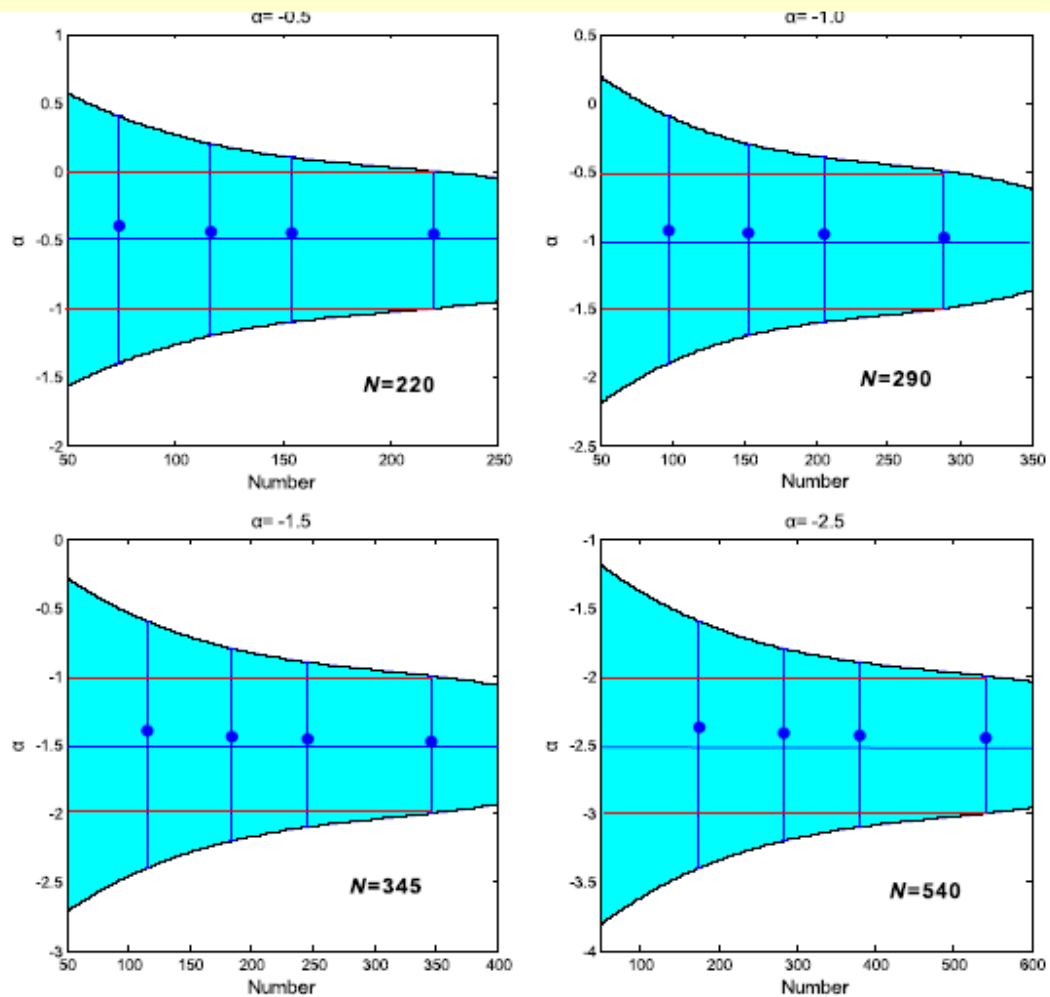


Figure 8. Evolution of the 95% confidence interval of α inferred from different simulated sample sizes. The black dotted line represents the true injected value and the red solid line is the two adjacent α values differing by 0.5. The black solid lines trace the averaged recovered confidence intervals, and the averaged most probable α values are marked with blue dots.

The expected detection rate of sGRBs

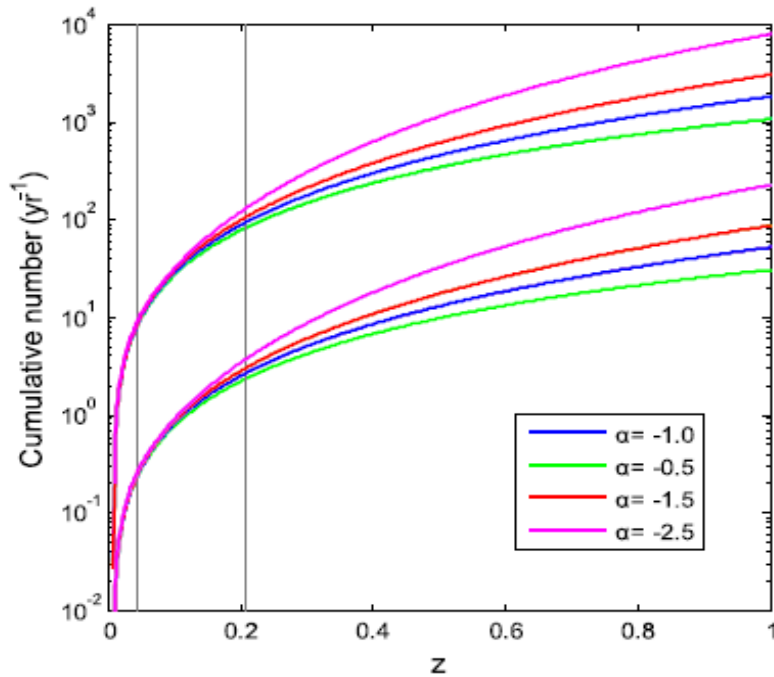


Figure 9. The expected detection rate of sGRBs with redshift. The solid and dotted lines represent the number of sGRBs with the rate of local NS-NS merger $110\text{--}3840 \text{ Gpc}^{-3} \text{ yr}^{-1}$ (Abbott et al. 2019). The two red lines represent the distances of 200 Mpc and 1 Gpc, respectively.

The Expected Detection Rate of sGRBs within Some Redshifts

Model	Redshift (distance)	The Expected Detection Rate (yr^{-1})
$\alpha = -0.5$	0.045(200 Mpc)	0.24 ~ 8.56
	0.208(1 Gpc)	2.35 ~ 82.06
	1	30.57 ~ 1069
$\alpha = -1.0$	0.045(200 Mpc)	0.25 ~ 8.82
	0.208(1 Gpc)	2.67 ~ 93.36
	1	52.08 ~ 1882.7
$\alpha = -1.5$	0.045(200 Mpc)	0.26 ~ 9.06
	0.208(1 Gpc)	3.01 ~ 105.36
	1	87.17 ~ 3050.6
$\alpha = -2.5$	0.045(200 Mpc)	0.27 ~ 9.48
	0.208(1 Gpc)	3.70 ~ 129.65
	1	225.88 ~ 7904.7

GECAM

Detection rate(yr^{-1})

Luminosity(ergs^{-1})

200Mpc

1.04 -35.96

6×10^{46}

1 Gpc

16.97 -593.91

4×10^{48}

Compare with observation

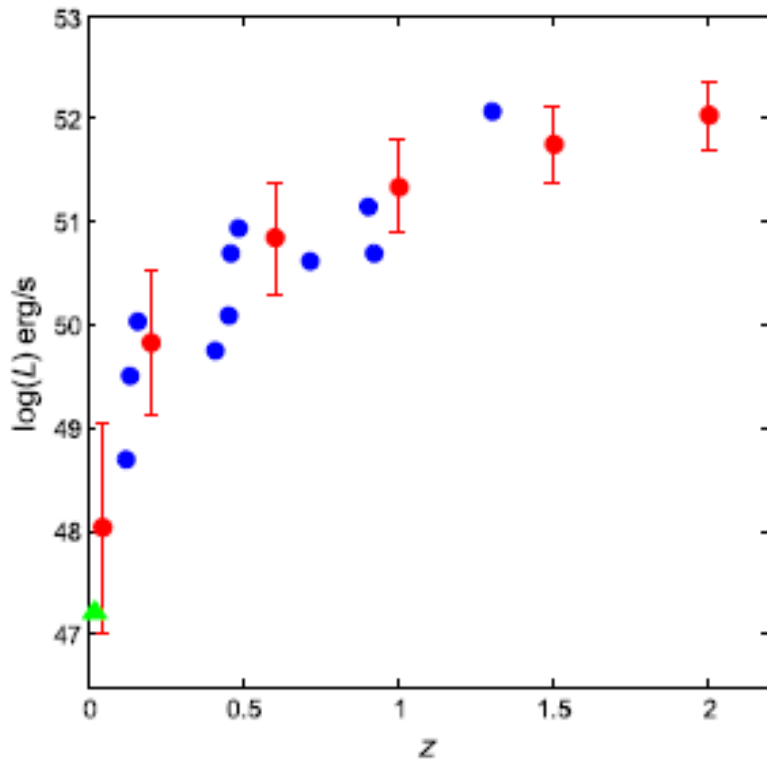


Figure 10. The relation between gamma-ray luminosity and redshift. The red circles represent our simulation results, the green triangle represents sGRB 170817A, and the blue circles are the sGRBs with known redshifts observed by Fermi-GBM (in Table 2). The error bars are 1σ errors.

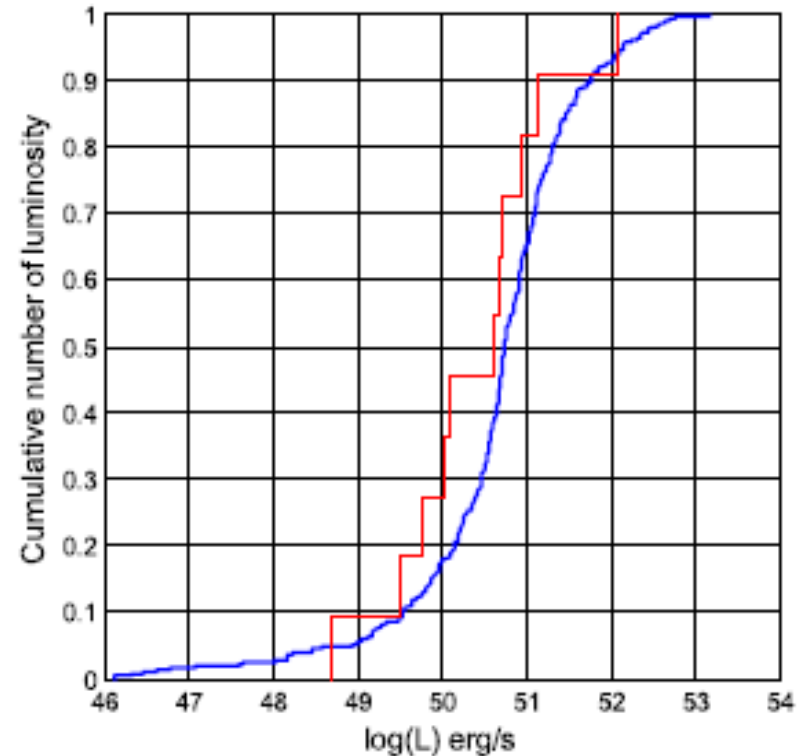
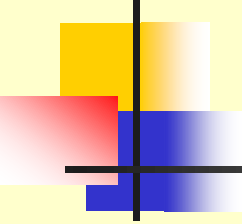
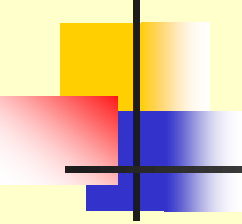


Figure 11. The cumulative luminosity distribution of our simulated sGRBs (blue line) and those with known redshifts (red line). The chance probability is 0.48.



Statistical properties of GRBs

- Two-parameter or three-parameter correlations:
- $E_p - E_{\text{iso}}$ (Amati et al.)
- $E_p - L_{\text{iso}}$ (Yonetoku et al.)
- $E_p - E_{\text{iso}} - t_{\text{break}}$ (Liang & Zhang)
- $E_p - L_{\text{iso}} - T_{0.45}$ (Firmani et al.)
-



Sample selections

- The redshift z
- The peak flux P and the peak fluence F
- The peak energy E_p
- Low-energy power-law index α and high-energy power-law index β of the Band function
- $T_{0.45}$

$E_p - L_{\text{iso}}$ & $E_p - E_{\text{iso}}$

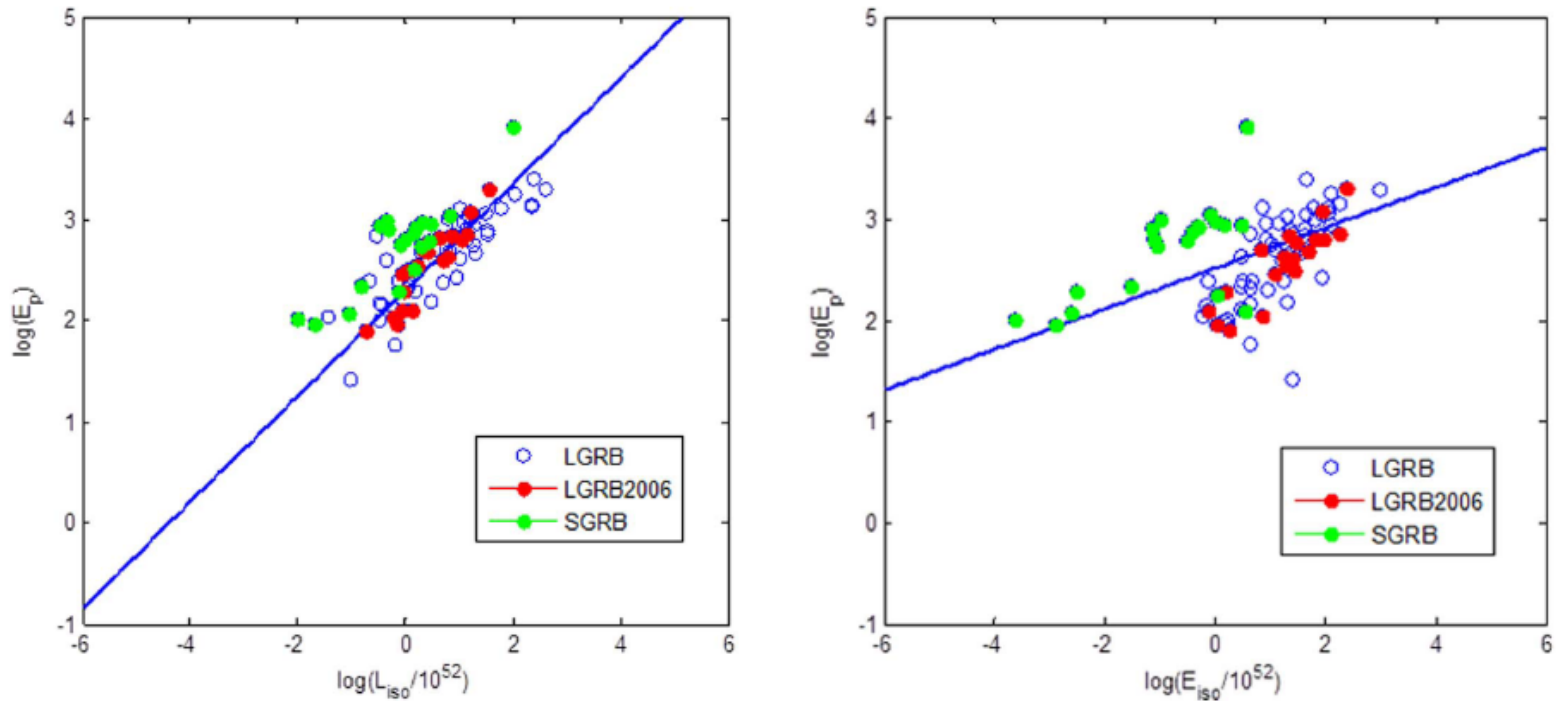


Figure 1. The $E_{\text{iso}} - E_{\text{peak}}$ and $L_{\text{iso}} - E_{\text{peak}}$ for LGRBs and SGRBs. The blue hollow points are the data for LGRBs in Table 1, the red solid points are the data for LGRBs in Firmani et al. (2006), and the green solid points are the data for SGRBs in table 2. The solid line is the best-fit line for LGRBs and SGRBs. The Spearman's rank correlation coefficients are $P = 0.71$ and $P = 0.46$ for the left and right panels, respectively.

(Guo, et al.2020)

$E_p - L_{\text{iso}} - T_{0.45}$ & $E_p - E_{\text{iso}} - T_{0.45}$

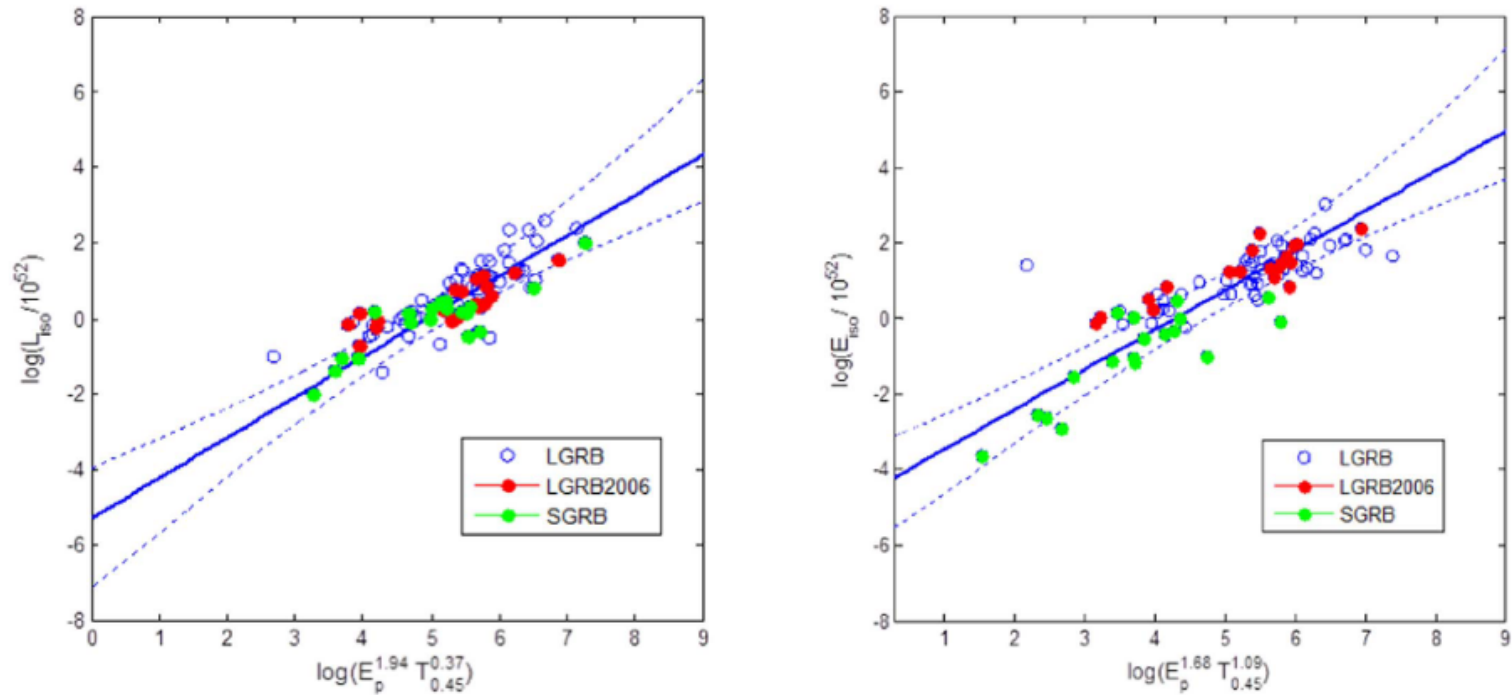


Figure 2. The three-parameter relations for LGRBs and SGRBs. The blue hollow points are the data for LGRBs in table 1, the red solid points are the data for LGRBs in Firmani et al. (2006), and the green solid points are the data for SGRBs in Table 2. The solid line is the best-fit line. The dotted lines represent the 3σ confidence bands. The Spearman's rank correlation coefficients are $P = 0.81$ and $P = 0.78$ for the left and right panels, respectively.

$$L_{\text{iso}} \propto E_{\text{peak}}^{1.94 \pm 0.06} T_{0.45}^{0.37 \pm 0.11}$$

$$E_{\text{iso}} \propto E_{\text{peak}}^{1.68 \pm 0.09} T_{0.45}^{1.09 \pm 0.13}$$

(Guo, et al.2020)

The scatter distribution

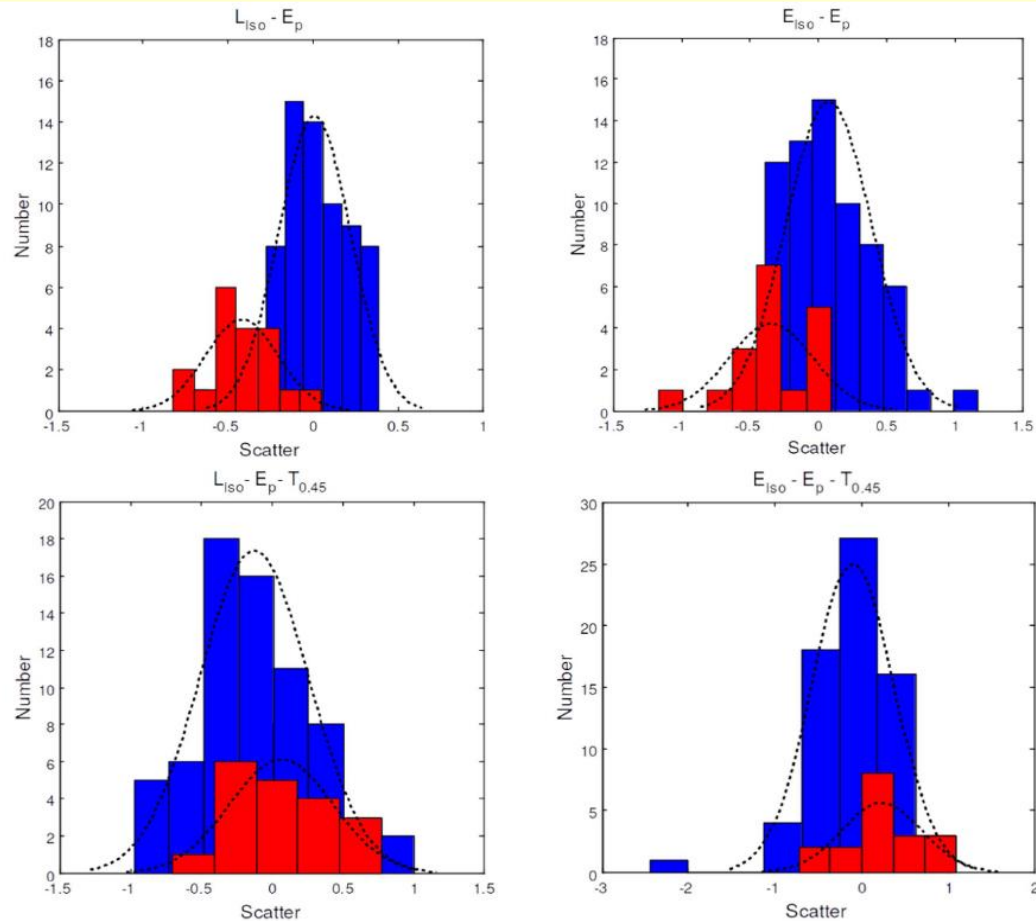


Figure 3. Left: the top graph shows the scatter with a Gaussian distribution of LGRBs and SGRBs for the $L_{\text{iso}} - E_{\text{peak}}$ relationship. The red represents the SGRBs' scatter with $\mu = -0.42$, $\sigma = 0.21$, and the blue represents the LGRBs' scatter with $\mu = 0.01$, $\sigma = 0.22$. The bottom graph shows the scatter of the LGRBs and SGRBs for the $L_{\text{iso}} - E_{\text{peak}} - T_{0.45}$ relationship. The red represents the SGRBs' scatter with $\mu = 0.06$, $\sigma = 0.37$, and the blue represents the LGRBs' scatter with $\mu = -0.12$, $\sigma = 0.38$. Right: the top graph shows the scatter with a Gaussian distribution of LGRBs and SGRBs for the $E_{\text{iso}} - E_{\text{peak}}$ relationship. The red represents the SGRBs' scatter with $\mu = -0.34$, $\sigma = 0.30$, and the blue represents the LGRBs' scatter with $\mu = 0.08$, $\sigma = 0.31$. The bottom graph shows the scatter of LGRBs and SGRBs for the $E_{\text{iso}} - E_{\text{peak}} - T_{0.45}$ relationship. The red represents the SGRBs' scatter with $\mu = 0.23$, $\sigma = 0.46$, and the blue represents the LGRBs' scatter with $\mu = -0.10$, $\sigma = 0.47$.

A new redshift indicator

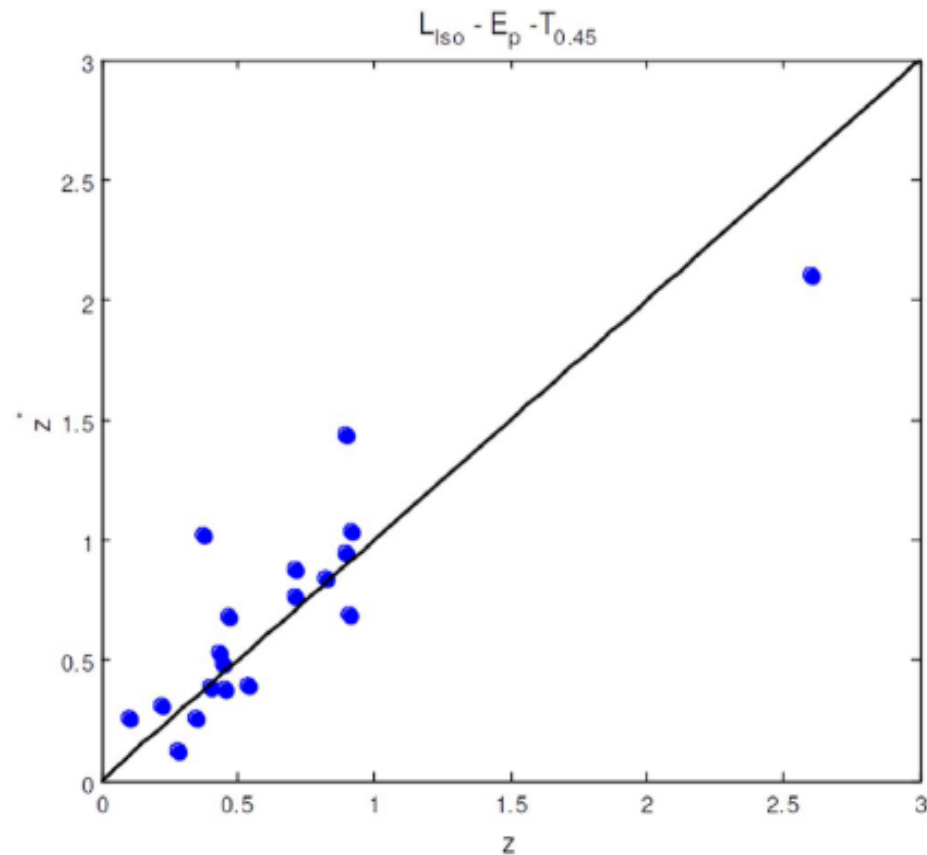


Figure 4. Comparison of real and pseudoredshifts of 19 short GRBs. The Y-axis is pseudoredshifts, and the X-axis is real redshifts.

Luminosity function & formation rate

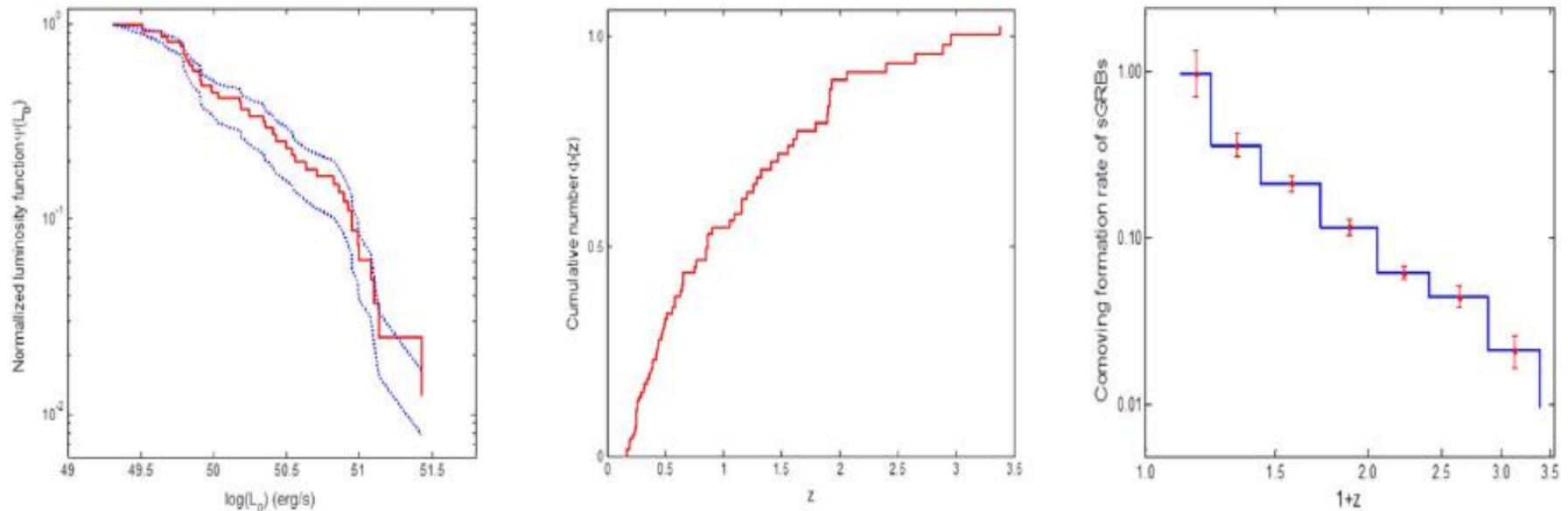
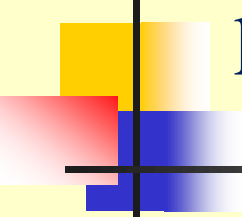
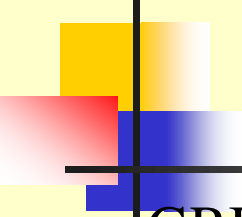


Figure 5. Left: cumulative luminosity function of SGRBs. The dotted lines are the 95% confidence bands (Moreira et al. 2010). Middle: cumulative redshift distribution of SGRBs. Right: the PDF of the redshift distribution derived from the cumulative distribution, with its first bin normalized to unity.



kilonova: transient from neutron star merger

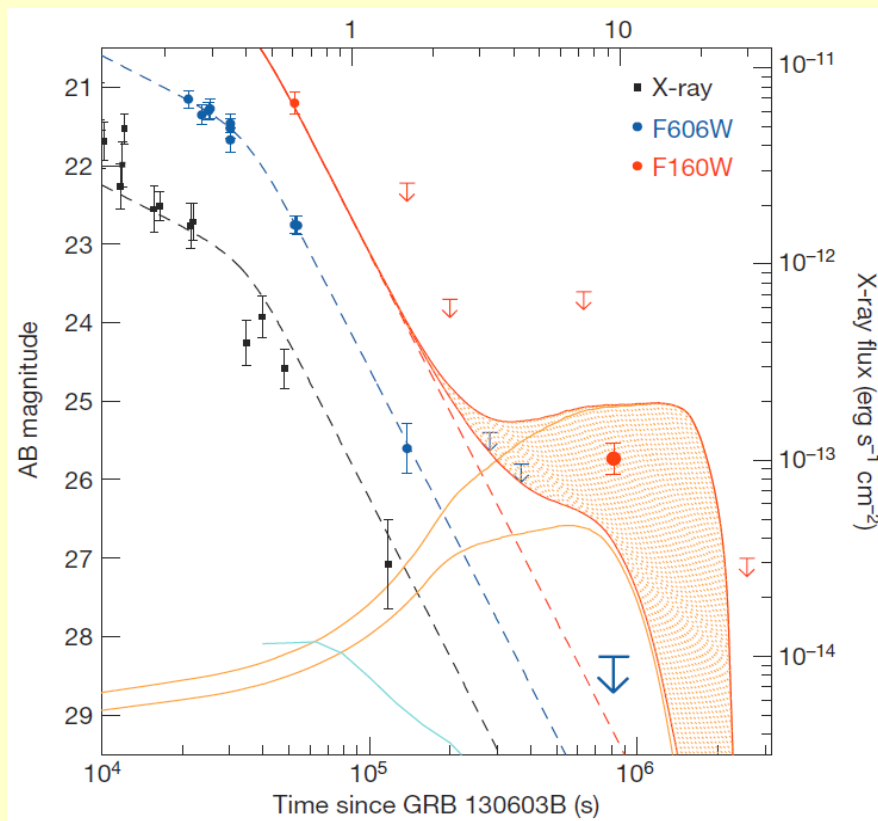
- Kilonova: Neutron star merger will produce an outflow dominated by r-process materials, the radioactive decay of the material will produce a supernova like transient (Li & Paczynski 1998).
- Merger-nova: if the merger remnant is a magnetar rather than a black hole, the spin-down power would enhance the kilonova emission (Yu et al. 2013, Gao et al. 2015, 2017)



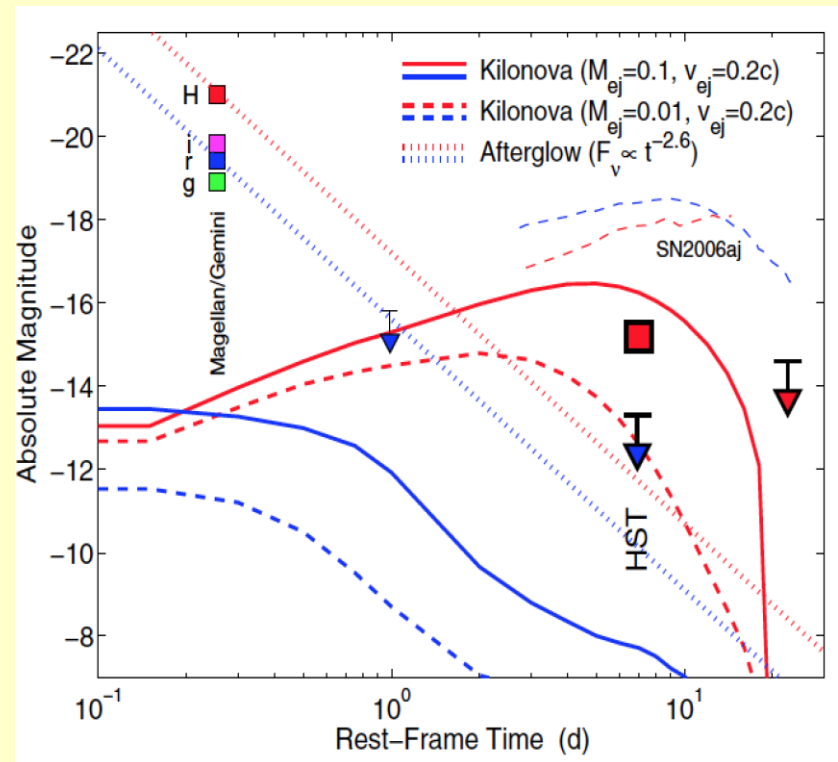
Known kilonova (candidates)

- GRB 130603B (Tanvir et al. 2013, Berger et al. 2013)
- **GRB 060614** (long-short GRB) (Yang et al. 2015, Jin et al. 2015)
- **GRB 050709** (Jin et al. 2016)
- AT2017gfo (...Pian et al. 2017, Covino et al. 2017, LIGO and Virgo et al. 2017...)
- GRB 150101B (Troja et al. 2018)
- **GRB 070809** (Jin et al. 2019)
- **GRB 160821B** (Jin et al. 2018, Gompertz et al. 2018, Troja et al. 2019, Lamb et al. 2019)

GRB 130603B: first kilonova signal

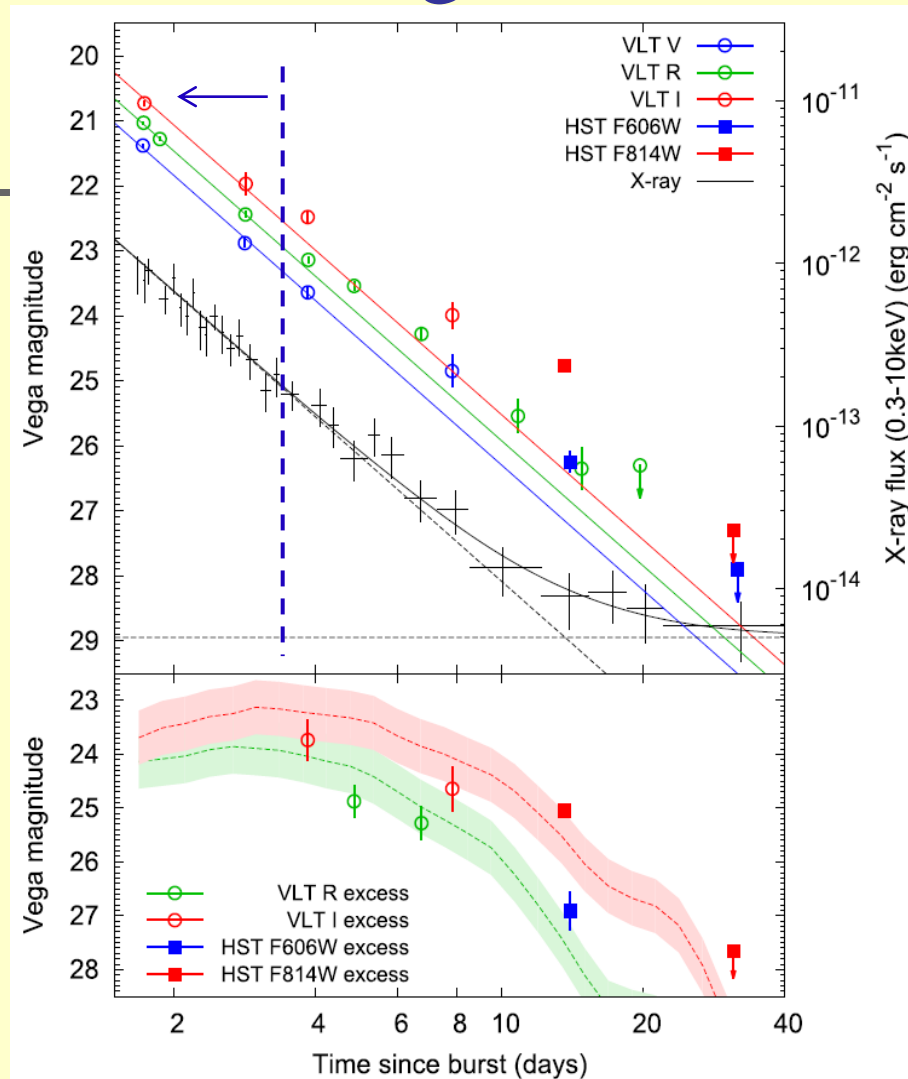


(Tanvir et al. 2013, Nature)



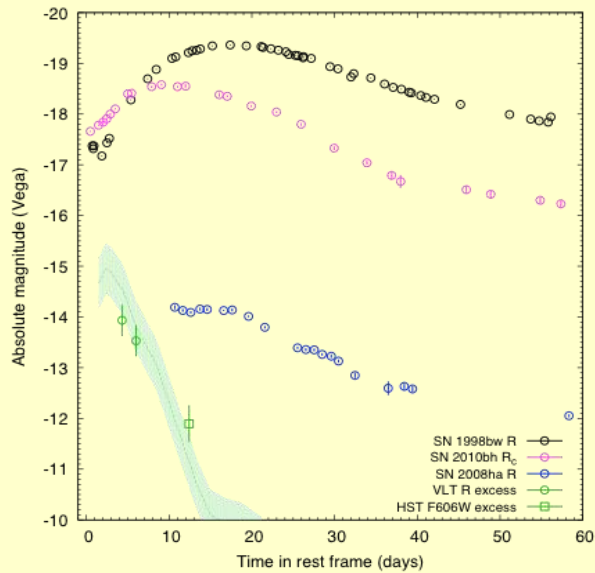
(Berger et al. 2013, ApJL)

GRB060614: first light curve of kilonova?

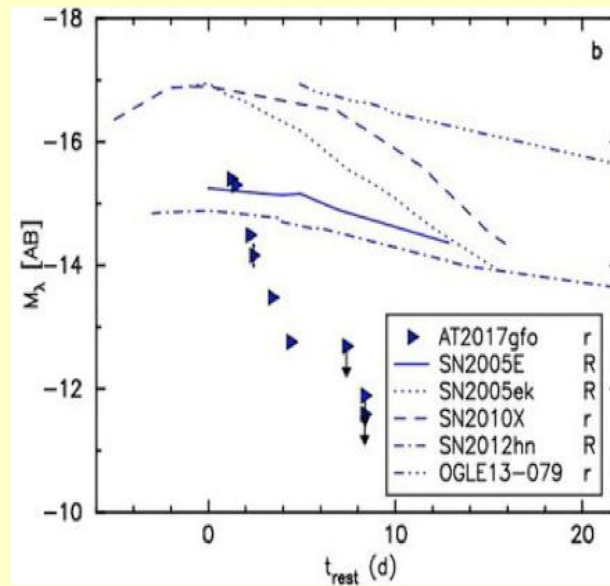


(Jin, Li & Cano et al. 2015 ApJL):

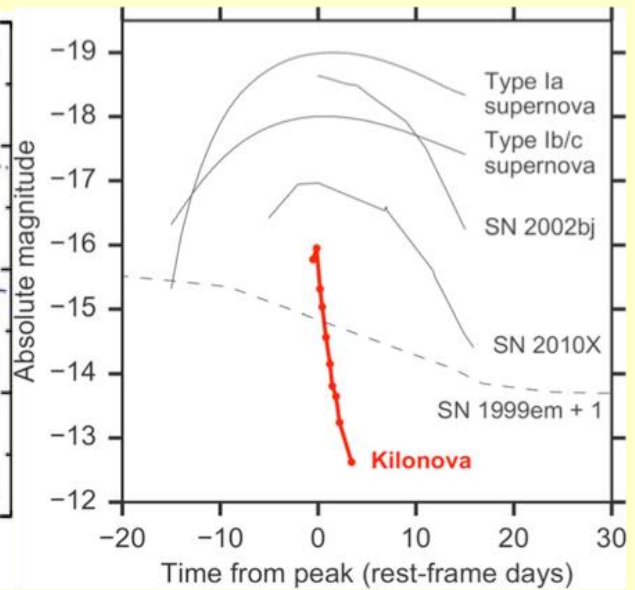
GRB 060614 & AT2017gfo vs. SNe



Jin et al. 2016 EPJWC



Smartt et al. 2017 Nature

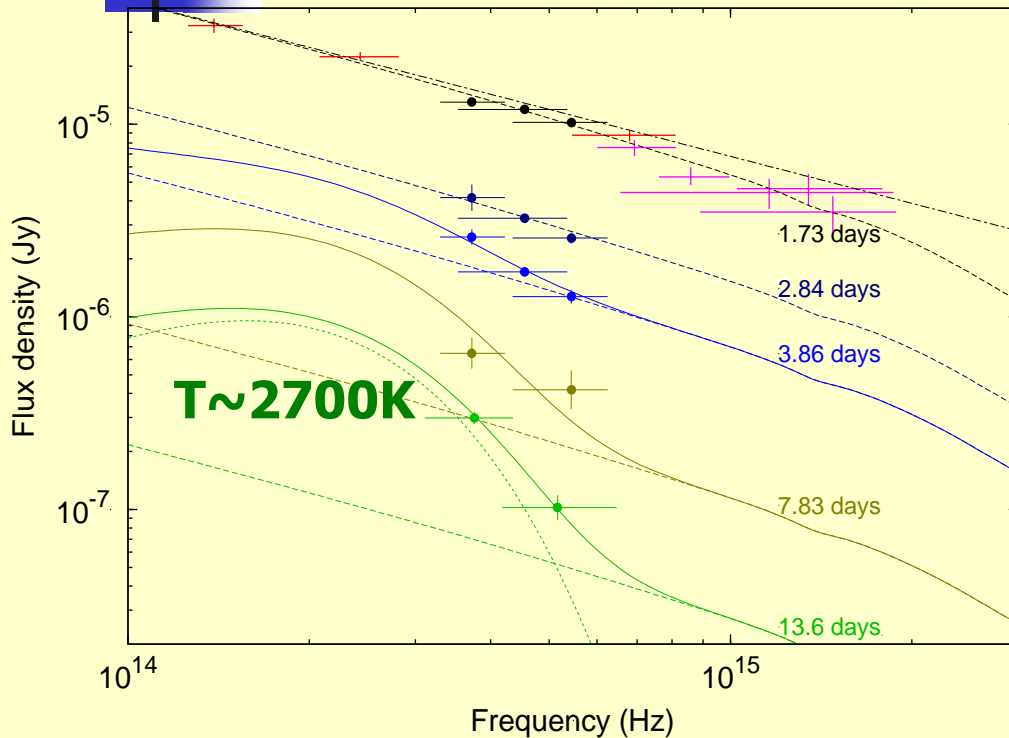


Arcavi et al. 2017 Nature

GRB 060614: first measurement of the (late time) temperature of kilonova?

GRB 060614

temperature $\sim 2700\text{K}$ @ 13.6 days

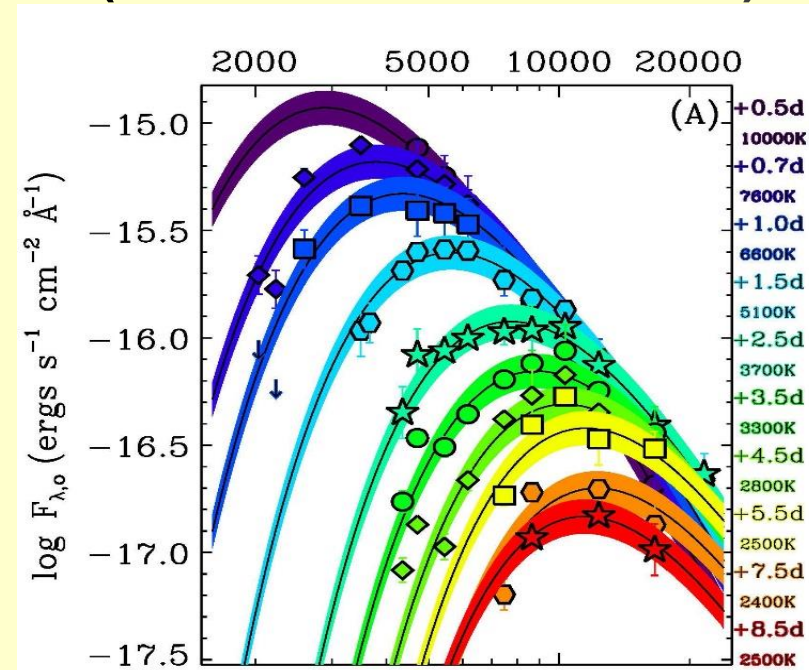


Jin et al. 2015 ApJL: at $t > 3.8$ days the emergence of a soft component

GW 170817

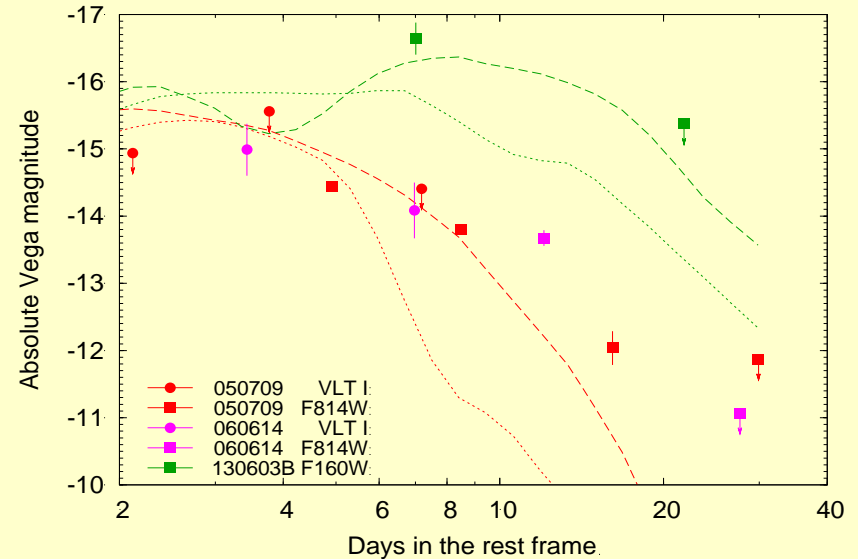
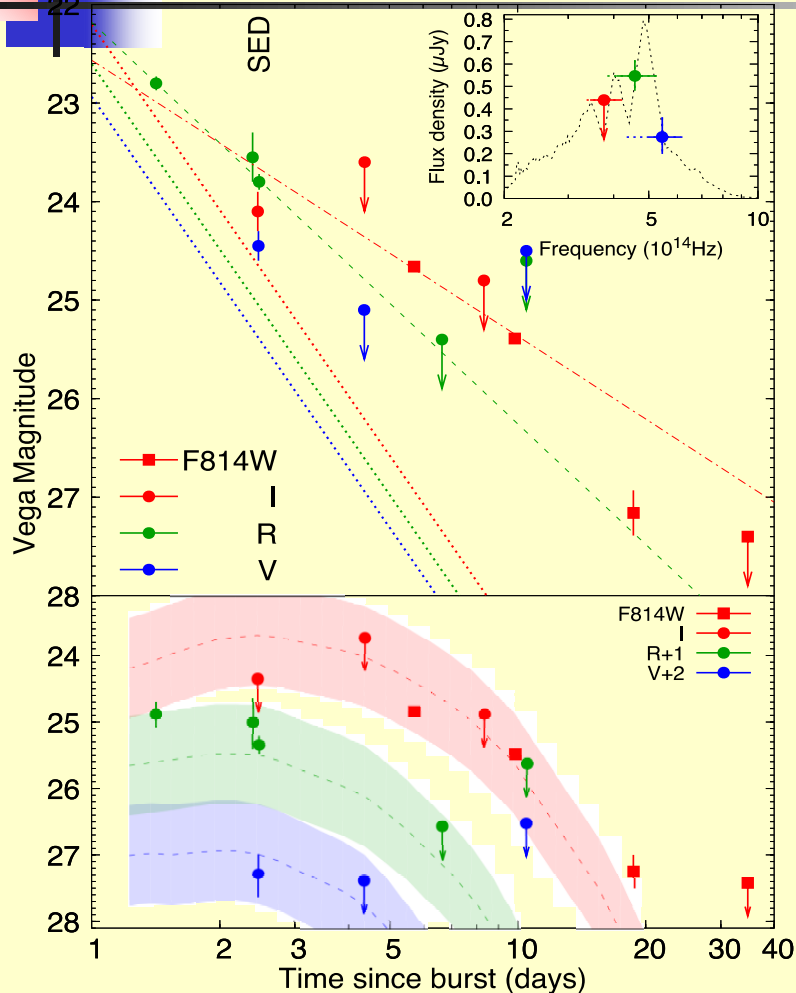
late temperature $\sim 2500\text{K}$

(Drout et al. 2017 Science)



A late time temperature of $\sim 2500\text{K}$

GRB 050709: kilonova signal



Left: The decline behaviors of I/F814W and R are significantly different!

Right: GRB 050709 I/F814W band light curve is similar to the kilonova of GRB 060614.

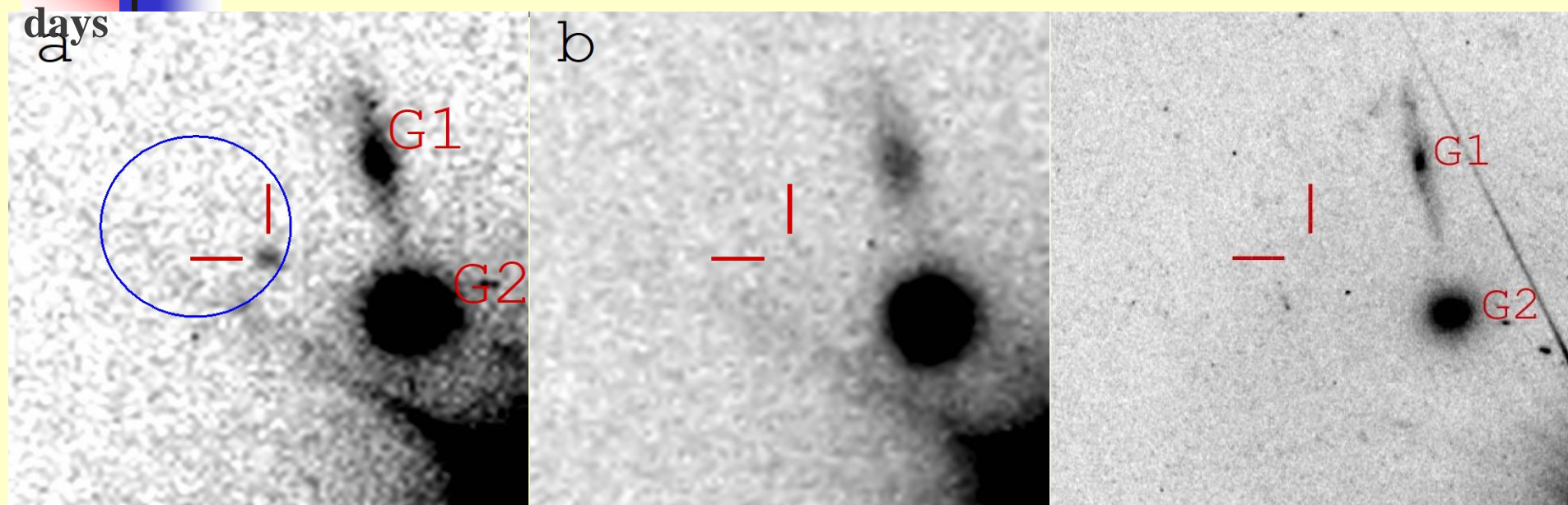
(Jin et al. 2016)

GRB 070809: limited but useful data

Keck R 0.5 day

Keck R 1.5 days

HST F606W 731

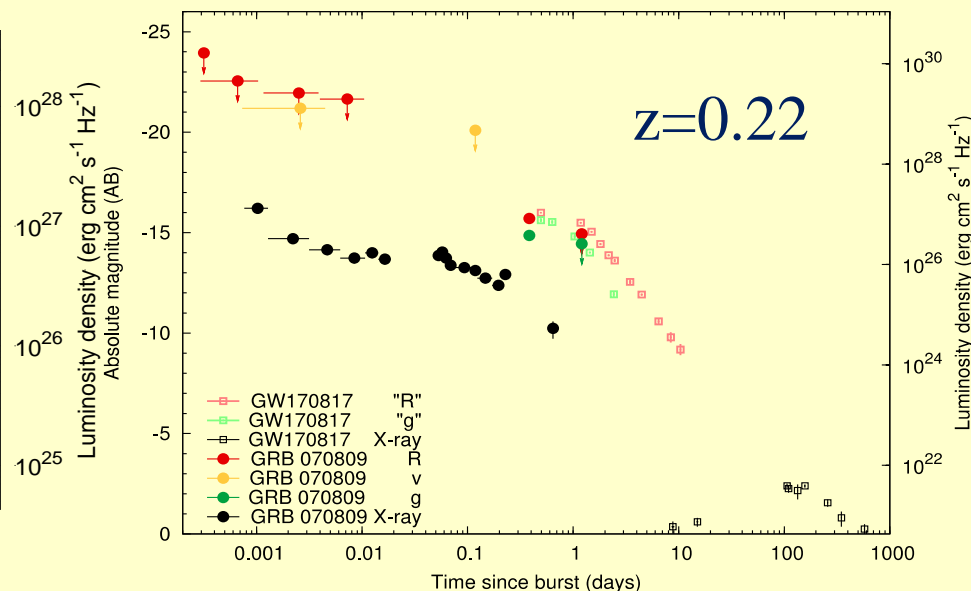
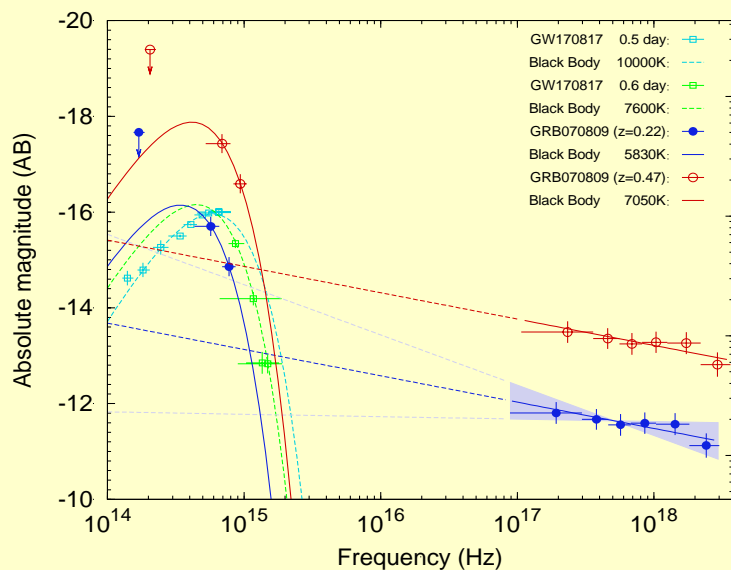


G1: $z=0.218$, offset 5.9 seconds (Perley 2008)

G2: $z=0.473$, offset 6.0 seconds (Berger 2010)

GRB site: $m(\text{F606W}) > 28.0$ AB mag

GRB 070809: spectra



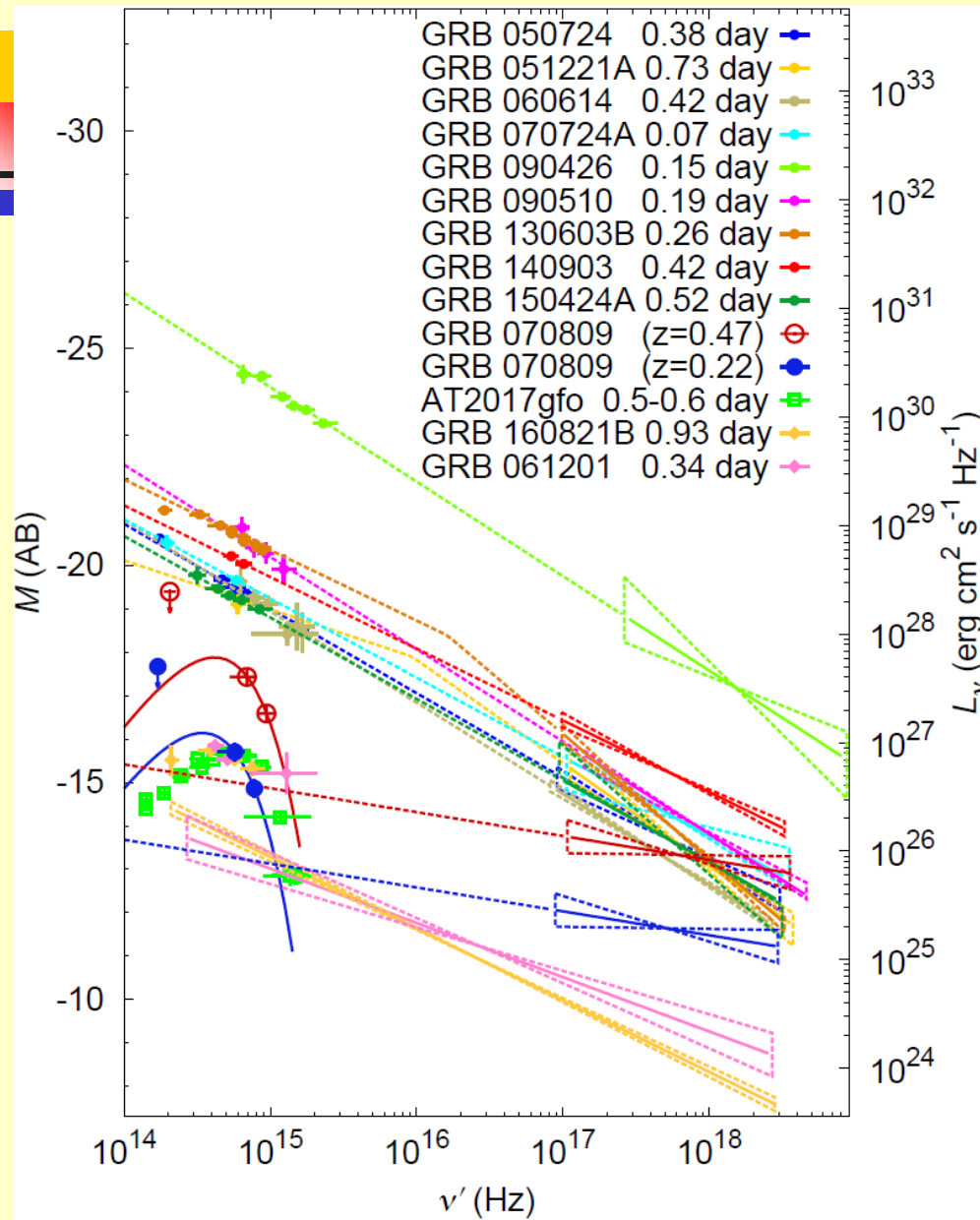
X-ray spectrum is very hard, the optical spectrum is very soft.

The kilonova emerge at early time ($t < 0.5$ day).

At $z=0.22$, the flux is close to GW170817, but the temperature is lower (5800K/7000K vs 10000K).

(Jin et al. 2020)

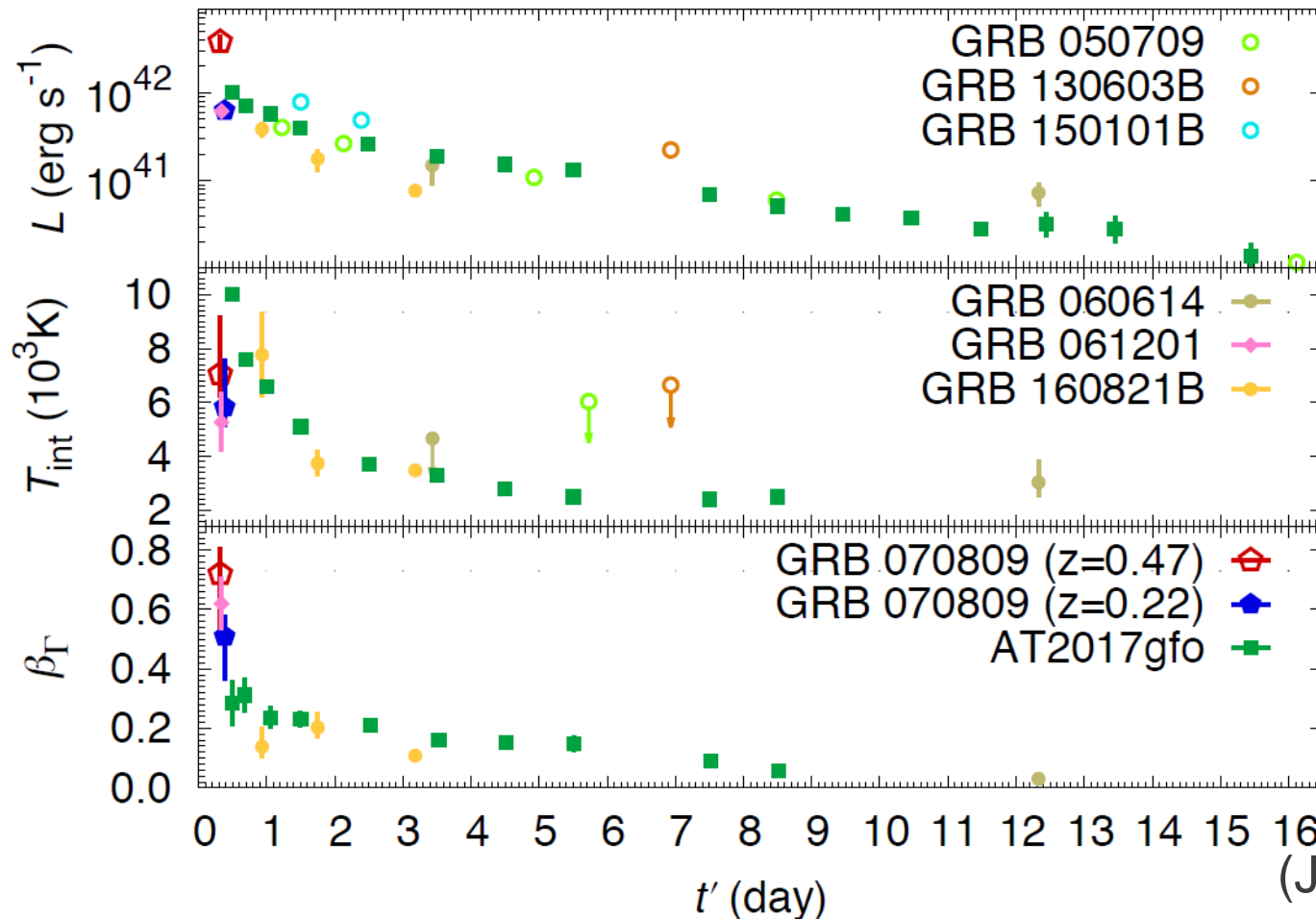
GRB 070809: the kilonova signal



Jin et al. (2020 Nat. Astron.):
GRB 070809 has the **hardest X-ray spectrum** and the **softest optical spectrum**.

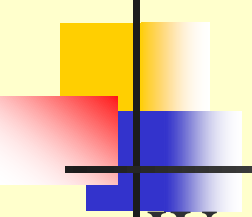
The **thermal-like optical emission** is well in excess of the extrapolation of the X-ray spectrum!

Statistical properties of kilonovae



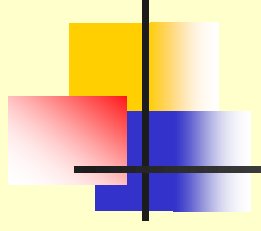
(Jin et al. 2020)

- The kilonova of GRB 070809 is the earliest one identified in “typical”/bright sGRBs.
- The early kilonova emission: diverse T_{int} , β_{Γ} and then diverse physical origins?



Summary

- We calculate the luminosity distribution of sGRBs and its evolution with redshift, for nearby sGRBs (luminosity distance less than 200Mpc) the typical luminosity is just around $10^{46} - 10^{47}$ ergs/s, the detection rate is about 1 yr^{-1} .
- We find a universal correlation that is suitable for both long and short GRBs.
- kilonova candidate: GRB 060614, GRB 050709, GRB 070809



Thank you!